Journal of Solid State Electrochemistry

Electrochemical analysis of gold embroidery threads from archaeological textiles

--Manuscript Draft--

Manuscript Number:	JSEL-D-18-00025R1
Full Title:	Electrochemical analysis of gold embroidery threads from archaeological textiles
Article Type:	Original Paper
Corresponding Author:	Antonio Domenech-Carbo University of Valencia Burjassot, Valencia SPAIN
Corresponding Author Secondary Information:	
Corresponding Author's Institution:	University of Valencia
Corresponding Author's Secondary Institution:	
First Author:	Antonio Domenech-Carbo
First Author Secondary Information:	
Order of Authors:	Antonio Domenech-Carbo
	Betlem Martínez, Graduate Restoration
	Joan Piquero-Cilla, Graduate Chemistry
	Noemí Montoya, PhD Chemistry
	María Teresa Doménech-Carbó, PhD Chemistry
Order of Authors Secondary Information:	
Funding Information:	MINECO (CTQ2014-53736-C3-1-P) — Prof. María Teresa Doménech-Carbó
	MINECO (CTQ2014-53736-C3-2-P) — Prof. Antonio Domenech-Carbo
	MINECO (CTQ2017-85317-C2-1-P) — Prof. María Teresa Doménech-Carbó
Abstract:	A methodology for characterizing archaeological gold embroidery threads based on two analytical techniques is described: Field emission scanning electron microscopy (FESEM-EDX) and voltammetry of immobilized microparticles methodologies (VIMP). After the analysis of the chemical composition of the metallic foil we analyse specific voltammetric features associated with the oxidation of gold in contact with aqueous H2SO4 and HCl electrolytes. Cyclic and square wave voltammetry (VMP) have been used to get information about the elemental composition and the corrosion products of the samples. AFM, FESEM-EDX and FESEM-FIB-EDX methodologies complete the study and brings us closer to the composition of the alloys and the embroidery manufacture techniques. This technique actualizes the VIMP data and evidences the morphological and elemental differences between them, in particular, it is confirmed that Au-Ag-Cu alloys, with notably differences in Ag content depending on the provenance, were used.
Response to Reviewers:	Reviewer #2: In page 6, line 8-10: Authors mentioned that under burial conditions gold could corrode leading to the pore formation. As authors explained later, this could be related to the dealloying of less noble metals than Au. Authors should also explain the effect of composition the samples on the pore formation (ChemCatChem 2013, 5, 2627 - 2635 and the references in that article). Response: In agreement with the kind suggestion of the reviewer, the text in page 6 has been extended in order to comment the pore formation associated to dealloying of

	less noble metals than Au. See marked text in page 6. The citation indicated by the reviewer and two other pertinent citations have been included as new references [44-46].

Electrochemical analysis of gold embroidery threads from archaeological textiles

Betlem Martínez[a,b], Joan Piquero-Cilla[a], Noemí Montoya[a], María Teresa Doménech-Carbó[b], Antonio Doménech-Carbó*[a]

[a] Departament de Química Analítica. Universitat de València. Dr. Moliner, 50, 46100 Burjassot (València) Spain.

[b] Institut de Restauració del Patrimoni. Universitat Politècnica de València. Camino de Vera 14, 46022, Valencia, Spain.

* Corresponding author, e-mail: antonio.domenech@uv.es.

Abstract

A methodology for characterizing archaeological gold embroidery threads based on two analytical techniques is described: Field emission scanning electron microscopy (FESEM-EDX) and voltammetry of immobilized microparticles methodologies (VIMP). After the analysis of the chemical composition of the metallic foil we analyse specific voltammetric features associated with the oxidation of gold in contact with aqueous H_2SO_4 and HCl electrolytes. Cyclic and square wave voltammetry (VMP) have been used to get information about the elemental composition and the corrosion products of the samples. AFM, FESEM-EDX and FESEM-FIB-EDX methodologies complete the study and brings us closer to the composition of the alloys and the embroidery manufacture techniques. This technique actualizes the VIMP data and evidences the morphological and elemental differences between them, in particular, it is confirmed that Au-Ag-Cu alloys, with notably differences in Ag content depending on the provenance, were used.

Keywords: Gilding; Voltammetry of microparticles; FESEM-FIB-EDX; AFM; Aging.

Introduction

Apart from its use for jewelry, cult figures, gold was also used since the antiquity in textiles [1,2]. The manufacturing technique of gilded metal embroidery threads used in the decoration of textiles suffered different variations [3,4] and was subject of imitations [5] making difficult their analytical characterization [6,7]. According to several authors [3,4,8-14], six main categories can be established for the use of metal in textiles in the past: a) metal applied to an already formed textile fabric by means of an adhesive, b) wires or strips of metal (lamellae) wound to a fiber core, c) the fiber core is wound with an organic (proteinaceous or cellulosic) wrapping at which is adhered the metallic surface, d) a gilt membrane strip is formed by beating on to an animal membrane (i.e. leather) thin gold sheets that are cut in narrow strips and wound to a fiber core e) strips of metal flattened or metal wires without a core fiber, and f) there is not fiber core and the organic strip is covered with the metallic surface fixed with an adhesive,. It is pertinent to emphasize that in the cases a) to d), the fibrous core has been reported to be made mainly of animal fibers (silk or wool), but also vegetal fibers (hemp or linen) [3,4], but the organic core is frequently lost so that metal threads appear as the principal remain. Therefore, characterization of the metal composition and micromorphology as well as fiber composition of metal embroidery is an important source of archaeological information.

A case study of particular interest is that represented by a series of gold embroidery threads from shrouds found in tombs of several archaeological necropolis of Valencia (Spain) currently under archaeological studies and conservation and restoration tasks by the *Servei d'Investigació Arqueològica Municipal de València* (SIAM). Four remains of gold embroidery textile corresponded to Islamic necropolis located in two archaeological sites of the historical center of Valencia (Spain) and other one was found in a necropolis dated on the Roman age [15,16].

In previous works, we have applied to voltammetry of immobilized particles (VIMP) methodology for studying mediaeval gildings in altarpieces [17] whose characterization [18,19], including the detection of falsifications [20] required trace analysis. The VIMP, a solid-state technique developed by Scholz et al. [21-23], is characterized by the requirement of amounts of sample at the nanogram level, thus having a minimally invasive character

prompting its application in the fields of archaeometry, conservation and restoration [24,25]. In line with previous on characterizing, authenticating and dating archaeological metals [26,27], this technique was applied, exploiting the widely studied electrochemistry of gold [28-39] and silver [40-43], for characterizing the aforementioned gilded embroidery threads in order to: i) electrochemically characterizing different manufacturing techniques, ii) discriminating pieces from different époques, and, iii) evaluating the incidence of aging processes.

The basic hypothesis is that the voltammetric response of gilded materials should be sensitive not only to changes in the chemical composition, the silver content and distribution as essential issue, but also to the textural properties (roughness, porosity) of the gilded surface, such properties being representative of the manufacturing technique and aging. The VIMP study was conducted upon attachment of nanosamples from gilding threads attached to graphite electrodes in contact with H_2SO_4 and HCl aqueous electrolytes and was complemented with morphological and compositional analyses performed with field emission scanning electron microscopy-X-ray microanalysis without (FESEM-EDX) and with use of focusing ion beam (FESEM-FIB-EDX.

Experimental

Description of the metal embroidery textile remains

Table 1 summarizes the characteristics of the series of archaeological remains of gold embroidery textile studied. All of them belong to the shrouds found in tombs of three archaeological necropolis of Valencia (Spain) currently under archaeological studies and conservation and restoration tasks by the *Servei d'Investigació Arqueològica Municipal de València* (SIAM). Three remains of gold embroidery textile studied corresponded to the shrouds found in three female burials at the *rawda* of the l'Almoina site (11^{th}-13^{th} century), the royal necropolis bound to the Islamic palace in the ancient city of *Balansiya* (currently Valencia) [15,16]. Other gold embroidery textile remain corresponded to another Islamic necropolis located in the archaeological site of *Roteros Alta* street in the historical center of Valencia, which presumed to be of the same age, and the later was of Roman age, providing

from the tomb 53 of a necropolis dated back to the 2th to 3th AD century. A fourth sample from the *Cisneros* street site in Valencia, dated back to the 18th century was also studied. Figure 1 depicts images of the remains **R.1**, **A.1**, **B.1**, **T.1** and **T.2**.

Description of gold embroidery thread samples

Samples analysed consisted of fragments of *at ca.* 3 mm of the gold embroidery threads from the different Valencian archaeological sites. As summarized in Table 2, all gold embroidery threads exhibit *S* twisted wrapping apart from Roman thread **R.1** that has *Z* twisted wrapping. All the gold embroidery threads exhibit a number of loops/mm in the range 3-5. Interestingly, some threads from site **T.1** are made using the technique of double gimped yarn that consist of use two gold strips that are subjected to twisted wrapping together.

Instrumentation and methods

Electrochemical experiments were performed in sample-modified graphite electrodes (Alpino HB, diameter 3 mm) at 298 K in a three-electrode cell under argon atmosphere using aqueous HCl and H_2SO_4 (Panreac reagents) solutions as supporting electrolytes. An AgCl (3 M NaCl)/Ag reference electrode and a platinum-wire auxiliary electrode completed the conventional three-electrode arrangement connected to a CH I660C equipment. Cyclic and square wave voltammetries (CV and SWV, respectively) were used as detection modes. For electrode modification, a thread fragment of ca. 0.5 mm length was placed on the plane face of an agate mortar and then the graphite electrode was pressed on it, using VIMP protocols [22-25]. The modified electrode was dipped into the electrochemical cell so that only the lower end of the electrode was in contact with the electrolyte solution in order to provide reproducible background currents.

Electron images of the surface of the threads and elemental composition was obtained with a Zeiss model ULTRA 55 field emission scanning electron microscope, which is coupled to an Oxford-X Max X-ray microanalysis system with an Aztec software. Secondary electron images were acquired at accelerating voltage of 2 kV. X-ray microanalysis was performed at 20 kV accelerating voltage and a working distance of 6-7 mm for the X-ray detector. A semiquantitative microanalysis was carried out by the ZAF method to correct interelemental effects. The counting time was 100 s. Presence of deposits of microcrystalline aggregates of

burial soil on the surface of the threads hindered the acquisition of X-ray spectra of the metal in large areas of the thread. Therefore, elemental composition of the metallic threads was obtained as the mean value of 3 point analysis performed on clean areas of the surface of the thread randomly selected. Relative error was maintained in all cases below 5%.

Cross sections of some threads were performed with a FIB-FESEM Zeiss (Orsay Physics Kleindiek Oxford Instruments) model Auriga equiped with a dual beam system that includes an electron beam and a Ga ion beam. The Ga beam impacts perpendicularly to the plane of the vertical wall of the trench by tilting the stage where is placed the thread 54º. The operating conditions were: voltage, 30 kV, current intensity, 500µA and 20 nA in the FIB for generating the focused beam of Ga ions. Secondary electron images of the trenches were performed in the FESEM operating with a voltage of 3 kV. Electron beam was optimally focused for acquiring images, which were automatically corrected by the software that performs a "tilt compensation". An Oxford-X Max X-ray microanalysis system coupled to the FESEM controlled by Aztec software was used for obtaining elemental compositions. A voltage of 20 kV and a working distance of 6-7 mm was used for acquiring X-ray spectra.

In situ AFM-monitored electrochemical experiments were performed with a multimode AFM (Digital Instruments VEECO Methodology Group, USA) with a NanoScope IIIa controller and equipped with a J-type scanner (max. scan size of 150×150×6 μm) using gold plates. 0.10 M H_2SO_4 was used as the electrolyte with Pt auxiliary and pseudo-reference electrode completing the three-electrode cell. The topography of the samples was studied in contact mode. An oxide-sharpened silicon nitride probe Olympus (VEECO Methodology Group, model NP-S) was used with a V-shaped cantilever configuration.

Results and discussion

FESEM-EDX and FESEM-FIB-EDX

Morphological characteristics of samples, obtained by FESEM-EDX examination, are summarized in Table 2. Figure 2a shows the secondary electron image of the Roman **R.1** sample of gold embroidery thread examined with the FESEM. The sample exhibits *Z* twisted wrapping of the flattened strips of gold characteristic of the Roman period. Figure 2b shows a

detail of the surface of the sample **R.1** in which is observed microcrystalline soil aggregates deposited on the metal surface. Absence of microstriations oriented in parallel to the direction of the thread suggest that the threads were made by beating gold to form sheets that were further cut in narrow strips. Pores of small size are also observed, probably formed owing to corrosion processes taking place as consequence of the exposure of the gold threads to the burial conditions. Such pores can be associated to the dealloying of less noble metals than Au, Ag and Cu in the studied threads. These features are consistent with pore formation in PtCu/C [44] and other [45,46] Pt-based bimetallic nanoparticles under the application of different potential inputs. Secondary electron images of samples **T.1.1**, **T.2** and **A.1** from the Islamic *l'Almoina* site are shown in Figures 2c and 3a,c, respectively. These flattened strips exhibit *S* twisted wrapping characteristic of the Islamic period. Interesting, sample **T.1.1** exhibits characteristic double gimped thread technique as is put in evidence in Fig. 2d in which the inner and outer gold strips can be observed. In the secondary electron image shown in Fig. 3b can be seen microstriations oriented in parallel to the direction of the thread. These features suggest that this thread was made by the cast, drawn and rolled technique. In contrast, sample **A.1** exhibited a smooth surface (Fig. 3d) that suggests that this thread was prepared by cutting of a gold flattened sheet. Similarly to samples **T.1.1** and **T.2**, Islamic sample **B.1** (Figs. 4a,b) from *Roteros-Alta* site showed microfeatures characteristic of cast, drawn and rolled technique.

Use of FESEM assisted by FIB provided secondary electron images of the cross section of the trenches performed on threads as it can be seen for sample **T.2** in Figure 4C as well as in depth concentration profiles (Figure 4D). These images have provided accurate measures of the thickness of the strips as is summarized in Table 2. In general, the strips analyzed exhibit strip thickness in the range 2.6-4.1 μm.

Table 3 summarizes the averaged values of element mass percentage for O, Cu, Ag, Au obtained by FESEM-EDX in the surface of the gold strips of embroidery textiles. The analyses performed on the surface of the threads confirm that, in all cases, the threads were prepared as Au-Ag-Cu alloy. Nevertheless, notable differences in composition were found between samples **R.1** and **A.1** and samples **T.1.1**, **T.1.2**, **T.2** and **B.1**. Thus, **R.1** and **A.1** threads exhibited an Au-rich composition with Au mass% up to 89% whereas samples **T.1.1**,

T.1.2, **T.2** and **B.1** exhibited high Ag contents ranging from 22.18% for sample **T.1.2.2** to 42.11% for sample **T.2**. The lowest copper content 0.8% was found in the Roman sample **R.1** whereas Islamic sample **B.1** exhibited the highest value of 2.37%. Small amounts of other elements such as C, Si or Al were also found in the surface of the thread. These elements are associated to the external deposits of microcrystalline aggregates of soil particles. Depth profiles could be performed in the trenches obtained in the threads that enabled the study of the variation of the composition of the alloy along the cross-section of the thread. As can be seen in Figure 4D for **T.2**, the content of Ag notably decreases in the outer 0.4 μm in both sides of the strip suggesting that corrosion processes taking place on the surface of the strips affect preferentially to this metal. Major content of Cu found in the surface also suggests that copper corrosion products could be formed in the surface of the thread.

Voltammetric features

Figure 5 compares the cyclic voltammetric response of sample **A.1** attached to graphite electrode and the bare electrode in contact with air-saturated 0.10 M HCl aqueous solution. The bare electrode displays a couple of high reversibility (anodic peak at +0.55 V (A_C), cathodic peak at +0.45 V vs. Ag/AgCl (C_C)) which can be associated to the presence of chloride in high concentration preceding the rising current at ca. +1.2 V associated to the oxygen evolution reaction (A_{OER}). In the region of negative potentials, a cathodic wave at ca. –0.5 V (C_{ox}), due to the reduction of dissolved oxygen, precedes the rising current for hydrogen evolution reaction (C_{HER}). The A_C/C_C couple can in principle be associated to oxygenated functionalities in the graphite surface [47,48], possibly also involved some chloride participation, as occurring in electrochemical intercalation of chloride into graphite [49,50]. The **A.1**-modified electrode showed a similar response, now dominated by an additional anodic peak at ca. +1.0 V (A_1) and the enhancement of the anodic current in the region around +0.8 V (A_2). The signals C_{ox} and, in particular, C_{HER} were also enhanced.

Figure 6 depicts the positive-going linear scan voltammograms (LSVs) a) **R.1**, b) **A.1**, c) **B.1** and d) **T.2** attached to graphite bars immersed into 0.10 M HCl. After semi-derivative convolution, peak resolution was increased and the signal A_1 and A_2 appeared as resolved peaks at ca. +1.0 (A_{11}) and +1.1 V (A_{12}) preceded by the background signal A_C and the peak A_2 at +0.80 V. A more or less intense anodic signal at +.011 V, attributable to silver oxidation

(A_{Ag}) was recorded. The voltammetric response in contact with 0.10 M H_2SO_4 was similar, although the gold-localized signals were of lower intensity than in the case of 0.10 M HCl electrolyte. Here, the gold-localized peak A_1 does not exhibit peak splitting while the signal A_2 looks like at least two superimposed peaks, as can be seen in Figure 7.

This electrochemistry can be described, following literature [28-39], on attributing the main anodic process A_1 to the electrochemical oxidation of metallic gold. In H_2SO_4 media a monolayer of various gold oxides is formed, a process which can be represented as:

$$Au_{\,solid} + 3H_2O \rightarrow Au_2O_{3\,solid} + 6H^+_{aq} + 6e^- \quad (1)$$

Accompanied, in HCl media, by the oxidative dissolution of gold to form Au(III)-chloride complexes. The electrochemical process appears to consist of a multi-step pathway involving chloride adsorption on gold and Au(I) and Au(III) complexes, the overall redox reaction being [51]:

$$Au_{\,solid} + xCl^-_{\,aq} \rightarrow AuCl_x^{(x-3)-}{}_{aq} + 3e^- \quad (2)$$

The appearance of two different anodic signals at ca. +1.0 (A_{11}) and +1.1 V (A_{12}) can be in principle attributed to the superposition of the oxidation processes of different crystalline planes of gold, a feature characterized in recent literature [28,34,39]. Finally, the signal A_2 can be attributed to the oxidation active surface sites (A*) associated to defect and/or coordinatively unsaturated sites [30,32,35,37] which can be represented as:

$$Au* \xrightarrow{-3e^-} Au^{3+} \xrightarrow{+(n+3)H_2O} Au^{3+}\cdot(n+3)H_2O \xrightarrow{-3H^+} Au(OH)_3\cdot nH_2O \quad (3)$$

At polycrystalline gold electrodes, surface active sites are electrochemically generated at cathodic potentials so that the signal only appears or becomes significantly enhanced after applying potentials more negative than ca. –0.2 V [23,25,29,32,43]. In agreement with prior observations on gildings [17] and natural gold [49], the signal A_2 appears in the voltammograms of gold threads without need of the above electrochemical activation, thus suggesting that such active sites have been generated during gold manufacturing.

The above electrochemical pathways can be considered as consistent with SEM images of graphite electrodes after abrasive transference of samples. Similarly to samples from gold of geological origin [52], isolated gold fragments excised from the thread appeared as irregular, laminated blocks of sizes between 5 and 10 μm adhered to the graphite substrate, as can be seen in Figure 8a, corresponding to a graphite bar after sampling on golden thread **T.1.1**, Consistently with previously described SEM data, mapping of Au and Ag yields a uniform distribution of both metals in the fragments (Figures 8b,c).

AFM examination of gold plates in contact with 0.10 M H_2SO_4 upon application of different potential inputs provides results in agreement with previous considerations. As can be seen in Figure 9, corresponding to AFM amplitude error channel graphs, the original gold surface shows an irregular faceting. After application of an oxidative potential step at +1.25 V during 5 min, the surface becomes smoothed and apparently enhanced as a result of the formation of the aforementioned gold oxide monolayer.

Gold embroidery characterization

Voltammograms in Figure 6 suggested that the different golden threads displayed distinct electrochemical responses. Since the amount of gold sample transferred onto the graphite electrode cannot be controlled, peak current ratios rather than absolute current values have to be used for characterizing the voltammetric responses. First of all, the ratio between the peak currents or peak areas of processes A_{Ag} and A_1, $i(A_{Ag})/i(A_1)$, can be considered as representative of the composition of the thread, thus denoting the more or less silvering of the gold. As far as the exposure of such different planes will be to a great extent determined by the thermomechanical treatment applied to the metal, the ratio between the peak currents (or peak areas) of signals A_{11} and A_{12}, $i(A_{11})/i(A_{12})$, should be representative of the differences in the manufacturing process. Similarly, the ratio between the peak currents for signal A_2, representative of active gold sites, and that of the signal A_1 (A_{11}, A_{12} and/or the two signals conjointly), $i(A_2)/i(A_1)$, could be representative of the specific manufacturing process.

Replicate experiments using freshly sample-modified graphite electrodes provided a satisfactory repeatability for each sample, the above peak current ratios varying within narrow ranges (*vide infra*). Figure 10 depicts the two-dimensional diagram corresponding to the

representation of the $i(A_{Ag})/i(A_{11}+A_{12})$ ratio vs. the $i(A_{11})/i(A_{12})$ ratio for the different studied golden threads taken the average values determined from three independent voltammetric measurements on sample-modified graphite electrodes under conditions such as in Figure 6.

Remarkably, the data points representative of samples **T.1.1**, **T.1.2**, **T.2** and **B.1** were characterized by relatively high $i(A_{Ag})/i(A_{11}+A_{12})$ ratios, being separated from the locations of data points for samples **A.1** and **R.1** characterized by weak A_{Ag} signals. However, no satisfactory correlation was obtained between the values of the $i(A_{Ag})/i(A_{11}+A_{12})$ ratio and the Ag/Au ratio determined by means of SEM/EDX analysis. This feature was possibly due to the variations in the silver content with depth (see Figure 4D) resulting in a relative enrichment of gold in the surface of threads.

In contrast with data for gold of geological origin [52], the ratio between the peak currents for the signals A_2 and $A_{11}+A_{12}$ produced relatively large differences between the different samples, being particularly enhanced in samples enriched in Ag (see Figure 6). This feature suggests that the presence of silver contributes to the creation of defect sites in the gold surface. This effect would be reinforced by the preferential release of surface silver upon corrosion previously described thus enhancing the accessibility of coordinatively unsaturated Au sites to the external, electro-responsive region of gold threads, as schematically depicted in Figure 11.

Figure 12 depicts a two-dimensional diagram representing the values of the $i(A_{11})/i(A_{12})$ ratio vs. those of $i(A_{11}+A_{12})$ again determined in voltammograms such as in Figure 6. In this diagram two or three replicate measurements on each golden thread are represented so that data points for sample **R.1**, of Roman age, defined a tendency curve whereas all other samples defined a common, different tendency curve. Taking into account that an increase of the value of the net $i(A_{11}+A_{12})$ current corresponds to the removal of more gold from deeper regions of the thread sample during the sampling process, the observed variations can be attributed to a variation of the contributions of the different crystal planes responsible for voltammetric signals A_{11} and A_{12} with depth. Attributing a chronological value to data in Figure 12, it is possible to suggest that Islamic threads, in principle dated between the 11^{th} and 13^{th} centuries (see Table 1) covered a relatively narrow period of time, their age being clearly different than

that of the Roman sample. However, as far as there are differences in the manufacturing process between the Roman and Islamic samples, the attribution of a chronological value to data in Figure 12 can only be merely tentative.

Conclusions

Using the voltammetry of immobilized particles methodology, attachment of submicrosamples from archaeological gold embroidery threads to graphite electrodes provided well-defined voltammetric responses in contact with aqueous H_2SO_4 and HCl solution. Signals for the oxidation of gold and silver were detected, the former consisting of anodic peaks attributable to the oxidation of gold in different crystalline planes and gold active sites. Voltammetric data, aided by AFM, FESEM/EDX and FESEM-FIB-EDX techniques, permitted to discriminate between different types of samples and suggested the possibility of obtaining chronological information.

Ackonwledgements: Projects CTQ2014-53736-C3-1-P and CTQ2014-53736-C3-2-P, which are supported with Ministerio de Economía, Industria y Competitividad (MINECO) and Fondo Europeo de Desarrollo Regional (ERDF) funds, as well as project CTQ2017-85317-C2-1-P supported with funds from, MINECO, ERDF and Agencia Estatal de Investigación (AEI) are gratefully acknowledged as well as the *Servei d'Investigació Arqueològica Municipal de València* (SIAM) for the access to the samples. The authors also whish to thank Dr. José Luis Moya López, Mr. Manuel Planes Insausti and Mrs. Alicia Nuez Inbernón (Microscopy Service of the Universitat Politècnica de València) for technical support.

References

[1] Járó M (2003). Metal threads in historical textiles, in Molecular and structural archaeology: Cosmetic and therapeutic chemicals, Centre de Recherche et de Restauration des Musées de France, Paris, pp 163–178

[2] Gleba M (2008) Auratae vestes: Gold textiles in the ancient Mediterranean, in Vestidos, Textiles y Tintes: Estudios sobre la produccion de bienes de consumo en la antigüedad, Proceedings of I Symposium Internacional sobre textiles y tintes del Mediterráneo en época romana, 2002. Consell Insular d'Eivissa i Formentera and Universitat de Valencia,pp 63–80

[3] Járó M (1990) Gold embroidery and fabrics in europe: XI–XIV centuries. Gold Bull 23: 40–57

[4] Karatzani A (2007). The evolution of a craft: the use of metal threads in the decoration of late and post Byzantine ecclesiastical textiles. University of London, London.

[5] Járó M (1995) Manufacturing technique of gold threads and their imitations on museum textiles-chronology of the preparation of metal threads. Results of the scientific investigations in Endrei W, Ed. Yearbook of the Textile Museum, Budapest, pp 31–51.

[6] Nord AG, Tronner K (2000). A note on the analysis of gilded metal embroidery threads. Stud Conservat 45:274–279

[7] Tronner K, Nord AG, Sjöstedt J, Hydman H (2002). Extremely thin gold layers on gilded silver threads. Stud Conservat 47:109–116

[8] Hoke E, Petrascheck-Heim I (1977). Microprobe analysis of gilded silver threads from mediaeval textiles. Stud in Conservat, 22:49–62.

[9] Indictor N, Koestler RJ, Blair C, Wardwell A (1988). The evaluation of metal warppings from medieval textiles using scanning electron microscoopy-energy dispersive X-ray spectrometry. Textile History 19:3–22.

[10] Indictor N, Koestler RJ, Wypyski M,Wardwell AE (1989). Metal threads made of proteinaceous substrates examined by scanning electron microscopy-energy dispersive x-ray spectrometry. Stud Conservat 34:171–182.

[11] Karatzani A (2006). Metal threads: the historical development. Proceedings ISA: 444.09–444.19.

[12] Járó M, Toth A, Gondar E (1990) Determination of the manufacturing technique of a 10th century metal thread. ICOM Committee for Conservation, 9th triennial meeting, Dresden, German Democratic Republic. ICOM Committee for Conservation, pp 299–301

[13] Enguita O, Climent-Font A, García G, Montero I, Fedi ME, Chiari M, Lucarelli F (2002). Characterization of metal threads using differential PIXE analysis. Nuclear Instruments and Methods in Physics Research B 189:328–333

[14] Balta ZI, Csedreki L, Furu E, Cretu I, Huszank R, Lupu M, Torok Z, Kertesz Z, Szikszai Z (2015). Ion beam analysis of golden threads from Romanian medieval textiles. Nuclear Instruments and Methods in Physics Research B 348:285–290

[15] Pascual-Pacheco J (1992) La necrópolis islámica de l'Almoina (Valencia). Primeros resultados. III CAME, Actas 2:406–412

[16] Pascual-Pacheco J, Serrano-Marcos ML (1996) Necrópolis islámicas en la ciudad de Valencia. Saitabi 46:231–252

[17] Ferragud-Adam X, Piquero-Cilla J, Doménech-Carbó MT, Guerola Blay V, Company X, Doménech-Carbó A (2017) Electrochemical analysis of gildings in Valencia Altarpieces: a cross-age study since 15th until 20th century. J Solid State Electrochem 21:1477–1487

[18] Constantinescu B, Vasilescu A, Radtke M, Reinholz U (2010) Micro-SR-XRF studies for archaeological gold identification—the case of Carpathian gold and Romanian museal objects. Appl Phys A 99:383–389

[19] Antonelli F, Lazzarini L, Cancellere S, Tesser E (2016) Study of the deteriortion products, gilding, and polychromy of the stones of the *Scuola Grande Di San Marco*'s façade in Venice, Stud Conserv 61:74–85.

[20] Gulotta D, Goidanich S, Bertoldi M, Bortolotto S, Toniolo L (2012) Gildings and false gildings of the baroque age: characterization and conservation problems. Archaeometry 54:940–954

[21] Scholz F, Meyer B (1998) Voltammetry of solid microparticles immobilized on electrode surfaces, Electroanalytical Chemistry, A Series of Advances. Bard AJ, Rubinstein I, Eds., Marcel Dekker, New York, vol. 20, pp 1–86

[22] Scholz F, Schröder U, Gulaboski R, Doménech-Carbó A (2014) Electrochemistry of Immobilized Particles and Droplets, 2nd Edit. Springer, Berlin-Heidelberg.

[23] Doménech-Carbó A, Labuda J, Scholz F (2013) Electroanalytical chemistry for the analysis of solids: characterization and classification (IUPAC Technical Report), Pure Appl Chem 85:609–631

[24] Doménech-Carbó A, Doménech-Carbó MT, Costa V (2009) Electrochemical Methods in Archaeometry, Conservation and Restoration. Monographs in Electrochemistry Series, Scholz F, Ed. Springer, Berlin-Heidelberg.

[25] Doménech-Carbó A (2010) Voltammetric methods applied to identification, speciation and quantification of analytes from works of art: an overview. J Solid State Electrochem 14:363–369

[26] Doménech-Carbó A (2011) Tracing, authentifying and dating archaeological metal using the voltammetry of microparticles. Anal Methods 3:2181–2188

[27] Burke LD, Nugent PF (1997) The electrochemistry of gold: I the redox behaviour of the metal in aqueous media. Gold Bull 30:43–53

[28] Chen A, Lipkowski J (1999) Electrochemical and Spectroscopic Studies of Hydroxide Adsorption at the Au(111) Electrode. J Phys Chem B 103:682–691

[29] Hoogvliet JC, van Bennekom WP (2001) Gold thin-film electrodes: an EQCM study of the influence of chromium and titanium adhesion layers on the response. Electrochim. Acta 47:599–611

[30] Burke LD, O'Mullane AP (2000) Generation of active surface states of gold and the role of such states in electrocatalysis. J Solid State Electrochem 4:285–297

[31] Burke LD, O'Mullane AP, Lodge VE, Mooney MB (2001) Auto-inhibition of hydrogen gas evolution on gold in aqueous acid solution. J Solid State Electrochem 5: 319–327

[32] Doyle RL, Lyons MEG (2014) The mechanism of oxygen evolution at superactivated gold electrodes in aqueous alkaline solution. J Solid State Electrochem 18:3271–3286

[33] Jeyabharathi C, Hasse U, Ahrens P, Scholz F (2014) Oxygen electroreduction on polycrystalline gold electrodes and on gold nanoparticle-modified glassy carbon electrodes. J Solid State Electrochem 18:3299–3306.

[34] Jeyabharathi C, Ahrens P, Hasse U, Scholz F (2016) Identification of low-index crystal planes of polycrystalline gold on the basis of electrochemical oxide layer formation. J. Solid State Electrochem 20:3025–3031

[35] Izumi T, Watanabe I, Yokoyama Y (1991) Activation of a gold electrode by electrochemical oxidation-reduction pretreatment in hydrochloric acid. J Electroanal Chem Interfacial Electrochem 303:151–160

[36] Scholz F, López de Lara González G, de Carvalho LM, Hilgemann M, Brainina Kh Z, Kahlert H, Jack RS, Minh DT (2007) Indirect Electrochemical Sensing of Radicals and Radical Scavengers in Biological Matrices. Angew Chem Int Ed 46:8079–8081

[37] Nowicka A, Hasse U, Sievers G, Donten M, Stojek Z, Fletcher S, Scholz F (2010) Selective Knockout of Gold Active Sites. Angew Chem Int Ed 49:3006–3009

[38] Hasse U, Fricke K, Dias D, Sievers G, Wulff H, Scholz F (2012) Grain boundary corrosion of the surface of annealed thin layers of gold by OH·radicals. J Solid State Electrochem 16:2383–2389

[39] Hasse U, Wulff H, Helm CA, Scholz F (2013) Formation of gold surfaces with a strongly preferred {100}-orientation. J Solid State Electrochem 17:3047–3053

[40] Cepriá G, Abadías O, Pérez-Arantegui J, Castillo JR (2001) Electrochemical behavior of silver-copper alloys in voltammetry of microparticles: a simple method for screening purposes. Electroanalysis 13:477–483

[41] Doménech-Carbó A, Doménech-Carbó MT, Pasíes T, Bouzas MC (2012) Modeling corrosion of archaeological silver-copper coins using the voltammetry of immobilized particles. Electroanalysis 24:1945–1955

[42] Capelo S, Homem PM, Cavalheiro J, Fonseca ITE (2013) Linear sweep voltammetry: a cheap and powerful technique for the identification of the silver tarnish layer constituent. J Solid State Electrochem 17:223–234

[43] Doménech-Carbó A, Del Hoyo-Meléndez JM, Doménech-Carbó MT, Piquero-Cilla J (2017) Electrochemical analysis of the first Polish coins using the voltammetry of immobilized particles. Microchem J 130:47–55

[44] Jeyabharathi C, Hodnik N, Baldizzone C, Meier JC, Heggen M, Phani KLN, Bele M, Zorko M, Hocevar S, Mayrhofer KJJ (2013) Time Evolution of the Stability and Oxygen Reduction Reaction Activity of PtCu/C Nanoparticles. ChemCatChem 5:2627–2635

[45] Meier JC, Galeano C, Katsounaros I, Topalov AA, Kostka A, Schuth F, Mayrhofer KJJ (2012) Degradation Mechanisms of Pt/C Fuel Cell Catalysts under Simulated Start–Stop Conditions. ACS Catal 2:832 –843

[46] Meier JC, Katsounaros I, Galeano C, Bongard HJ, Topalov AA, Kostka A, Karschin A, Schuth F, Mayrhofer KJJ (2012) Stability investigations of electrocatalysts on the nanoscale. Energy Environ Sci 5:9319 –9330

[47] Martí-Villaba M, Davis J (2008) New directions for carbon-based detectors: exploiting the versatility of carbon substrates in electroanalysis. J Solid State Electrochem 12:1245–1254

[48] Noked M, Soffer A, Aurbach D (2011) The electrochemistry of activated carbonaceous materials: past, present, and future. J Solid State Electrochem 15:1563-1578

[49] Kang F, Leng Y, Zhang T-Y, Li B (1998) Electrochemical synthesis and characterization of ferric chloride-graphite intercalation compounds in aqueous solution. Carbon 36:383-390

[50] Urbaniak J, Skowronski JM, Olejnik B (2010) Preparation of Fe_2O_3-exfoliated graphite composite and its electrochemical properties investigated in alkaline solution. J Solid State Electrochem 14:1629–1635

[51] Herrera-Gallego J, Castellano CE, Calandra AJ, Arvia AJ (1975) The electrochemistry of gold in acid aqueous solutions containing chloride ions. J Electroanal Chem 66:207–230

[52] Doménech-Carbó A, Scholz F, Schmitt RT, Usera J, García-Forner AM, De la Fuente-Arévalo, Jeyabharathi C, Piquero-Cilla J, Montoya N (2017) Electrochemical characterization

of natural gold samples using the voltammetry of immobilized particles. Electrochem Commun 85:23–26

Table 1. Description of samples in this study.

Simple/Code	Period/ Site/(date of recovery)	Description
R.1 MIS004 U.E. 1389	Roman (2^{nd}-3^{rd} DC)/ Misericordia/Cañete (1994)	Fragments of gimped threads with maximum length *at ca* 2-3 mm, found among remains of sediments. The threads are flattened strips. No textile fabric was found. The gold embroided textile was associated to head and thorax. Archaeological remains analysed no treated
A.1 1ALM000U.E. 1464	Islamic (11^{th} century)/ L'Almoina (1987)	Fragments of embroided textile of 30 cm length and 5 cm width. Threads with rests of sediments grouped forming parallel gold strips. The threads are flattened strips with maximum length *at ca* 3 mm. The tomb belongs to a female deceased and the gold embroided textile was associated to the thorax. Restoration process in 1989. Archaeological remains analysed no treated.
T.1 1ALM00 U.E. 10789	Islamic (11^{th}-13^{th} century)/ L'Almoina (1987)	Fragments of threads detached of the sediments. The threads are simple (sample T.1.1) and double (sample T.1.2) gimped flattened strips with maximum and minimum length *at ca* 5 and 2 mm, respectively. The tomb belongs to a female deceased and the gold embroided textile is associated to the head. No treated.
T.2 1ALM00 U.E. 10793	Islamic/L'Almoina (2001)	Eleven fragments of embroided textile grouped forming parallel gold strips and spirals with area in the range 1-6 mm^2 and detached gold threads. The threads are flattened strips. The tomb belongs to a female deceased. Restoration process in 2002. Archaeological remains analysed no treated.
B.1 ALTA48 U.E. 2318	Islamic/ Roteros-Alta 48-58 (1997)	Fragments of disaggregated gimped threads with remains of soil of the tomb. The threads are flattened strips. Fragments of threads. Archaeological remains analysed no treated.

Table 2. Morphological characteristics of the gold embroidery threads.

Sample	Thickness (μm)	Width of strip (μm)	Width of thread (μm)	Loops/mm	Twisted wrapping
R.1	-	310	215-190	4	Z
A.1	-	330	210-150	5	S
T.1.1	4.1	410	-	3	S
T.1.2	4.0	320	350-570	3	S
T.2	3.4	410	370	3	S
B.1	2.6	490	420-440	5	S

Table 3. Chemical composition (elemental weight %) obtained in the surface of the gold strips of the samples of gold embroidery textile using FESEM-FIB-EDX. The sample **T.1.2** is a double gimped thread; sample **T.1.2.1** is the outer strip in the double gimped strip, sample **T.1.2.2** is the inner strip in the double gimped strip that originally was in contact with the fiber core.

Element	R.1	A.1	T.1.2.1	T.1.2.2	T.2	B.1
Au	89.50	94.54	62.02	73.19	52.01	58.23
Ag	7.2	2.46	32.98	22.18	42.11	35.50
Cu	0.8	1.79	0.93	0.41	-	2.37
O	2.5	1.01	3.86	3.73	1.2	0.75

*

Figures

Figure 1. Photographic images of the: A) Roman remains **R1**; B) Islamic remains **B1**; C) Islamic remains **A1**; D) Islamic remains **T2**; E) Islamic remains **T1.**

Figure 2. Secondary electron image of: A) sample of gold gimped strip **R.1**; B) detail of the surface of sample **R.1**; C) sample of double gimped strip **T.1.2**; D) detail of the double gimped strip in sample **T.1.2**.

Figure 3. Secondary electron image of: A) sample of gold gimped strip **T.2**; B) detail of the surface of sample **T.2**; C) sample of gold gimped strip **A.1**; D) detail of the surface of sample **A.1**.

Figure 4. Secondary electron image of: A) sample of gold gimped strip **B.1**; B) detail of the surface of sample **B.1**; C) secondary electron image of the trench performed with FESEM-FIB in sample **T.2**; D) x-ray linescan carried out in sample **T.2** providing depth profile of elemental composition along the trench.

Figure 5. Cyclic voltammogram of sample **A.1** (black line) attached to graphite bar immersed into 0.10 M HCl superimposed to the voltammogram at the bare electrode (red line). Potential scan initiated at 0.0 V in the positive direction; potential scan rate 50 mV s^{-1}.

Figure 6. Linear potential scan voltammograms of samples a) **R.1**, b) **A.1**, c) **B.1** and d) **T.2** attached to graphite bars immersed into 0.10 M HCl. Potential scan initiated at –0.25 V in the positive direction; potential scan rate 50 mV s^{-1}. Semi-derivative convolution of data was applied to increase peak resolution.

Figure 7. Linear potential scan voltammograms of samples a) **R.1**, b) **A.1**, c) **B.1** and d) **T.2** attached to graphite bars immersed into 0.10 M H_2SO_4. Potential scan initiated at –0.25 V in the positive direction; potential scan rate 50 mV s^{-1}. Semi-derivative convolution of data was applied to increase peak resolution.

Figure 8. a) SEM image of a graphite electrode after sampling on thread **T.1.1**, and b) gold and c) silver mapping.

Figure 9. AFM examination of a gold plate in contact with 0.10 M H_2SO_4 a,b) before and c,d) after application of an oxidative potential step at +1.25 V during 5 min. a,c) Amplitude error channel graphs; b,d) topographic profiles along the lines marked with white double arrows.

Figure 10. Two-dimensional diagram plotting the $i(A_{Ag})/i(A_{11}+A_{12})$ ratio vs. the $i(A_{11})/i(A_{12})$ ratio for golden threads in this study. Averaged data from three independent voltammetric measurements under conditions such as in Figure 6.

Figure 11. Scheme for describing the increase in the relative proportion of active gold sites in gold embroidery threads containing high silver content.

Figure 12. Two-dimensional diagram for the values of the $i(A_{11})/i(A_{12})$ ratio represented as a function of $i(A_{11}+A_{12})$ determined in voltammograms such as in Figure 6. Two or three replicate measurements on each golden thread are represented. Tentative tendency lines are presented from the potential fit of experimental data.

Figure 1.

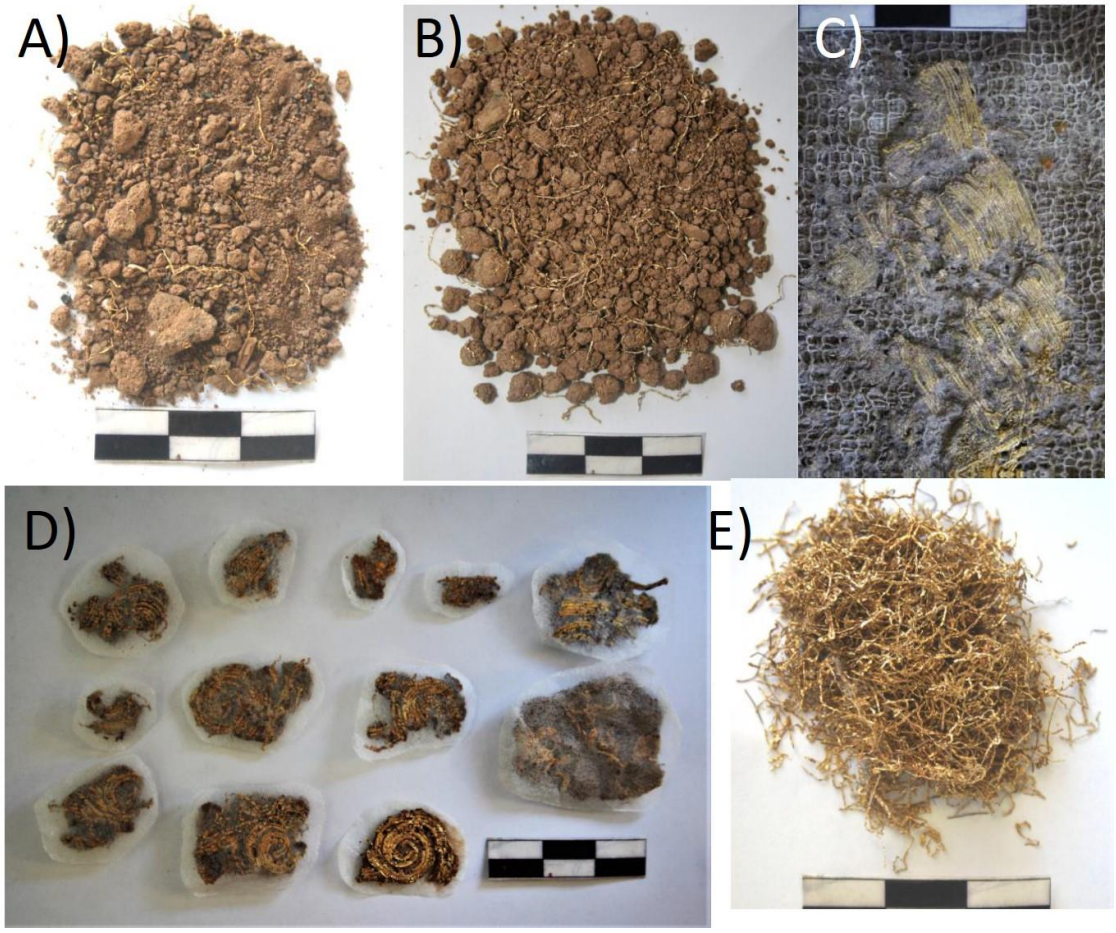

Figure 2.

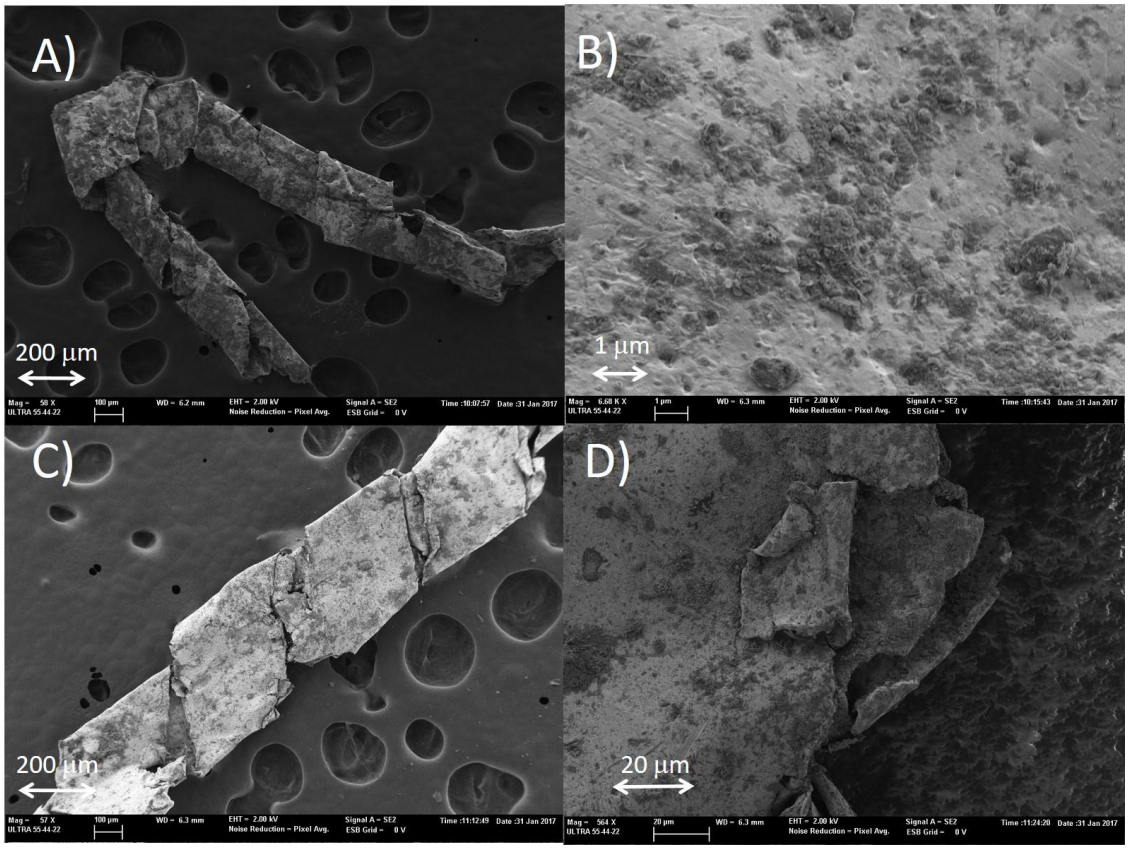

Figure 3.

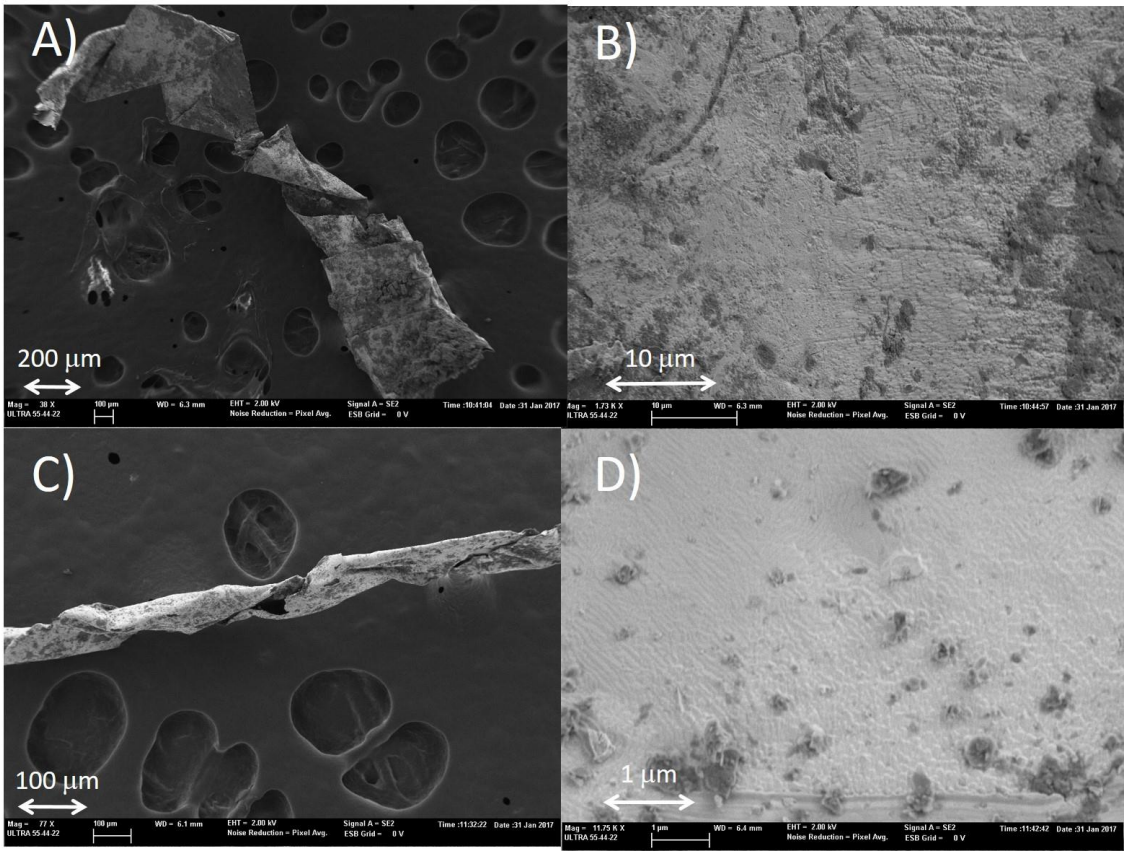

Figure 4.

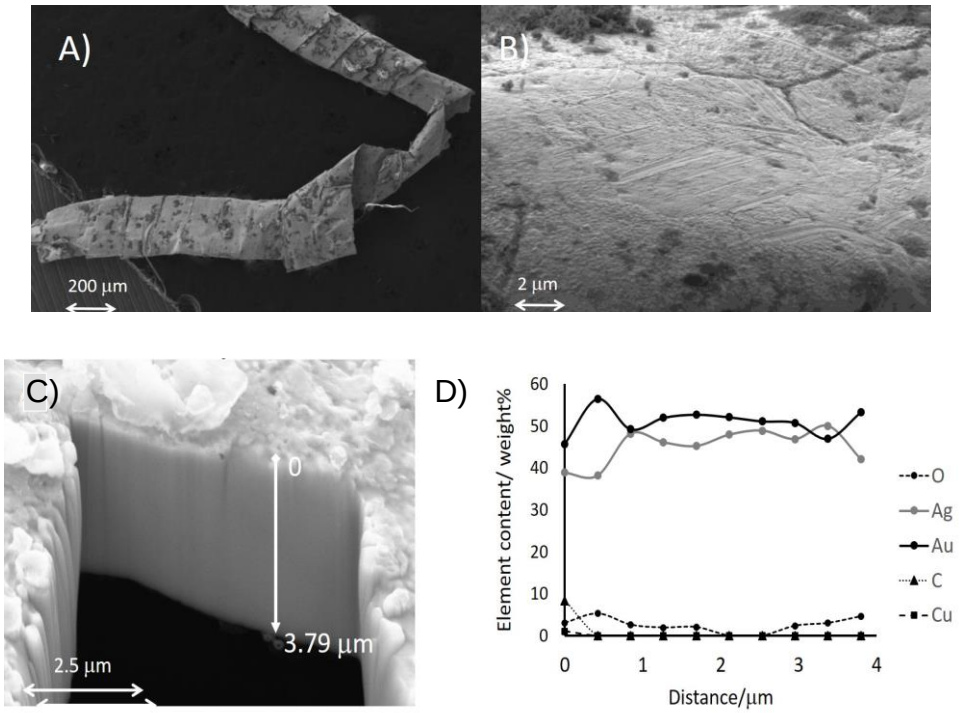
A)
200 µm
B)
2 µm
C)
0
3.79 µm
2.5 µm
D)
Element content/ weight%
60
50
40
30
20
10
0
0
1
2
3
4
Distance/µm
O
Ag
Au
C
Cu

Figure 5.

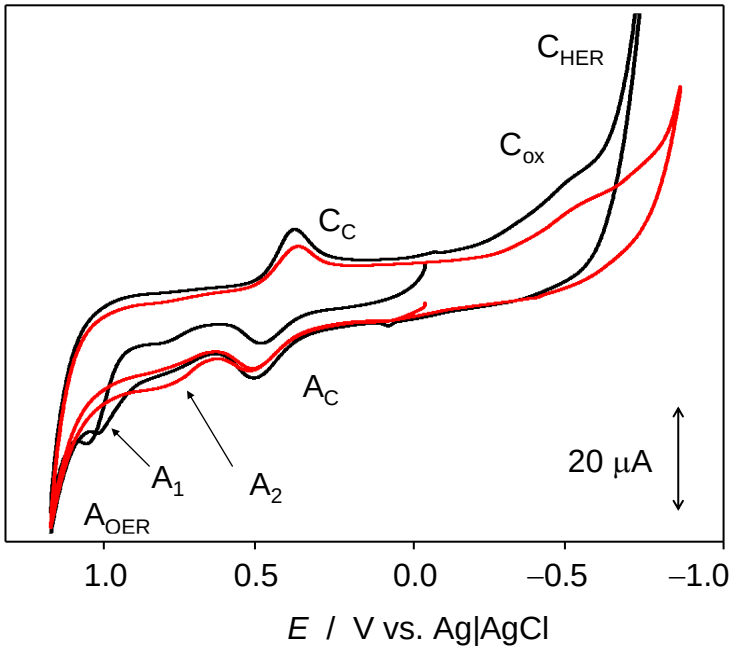

Figure 6.

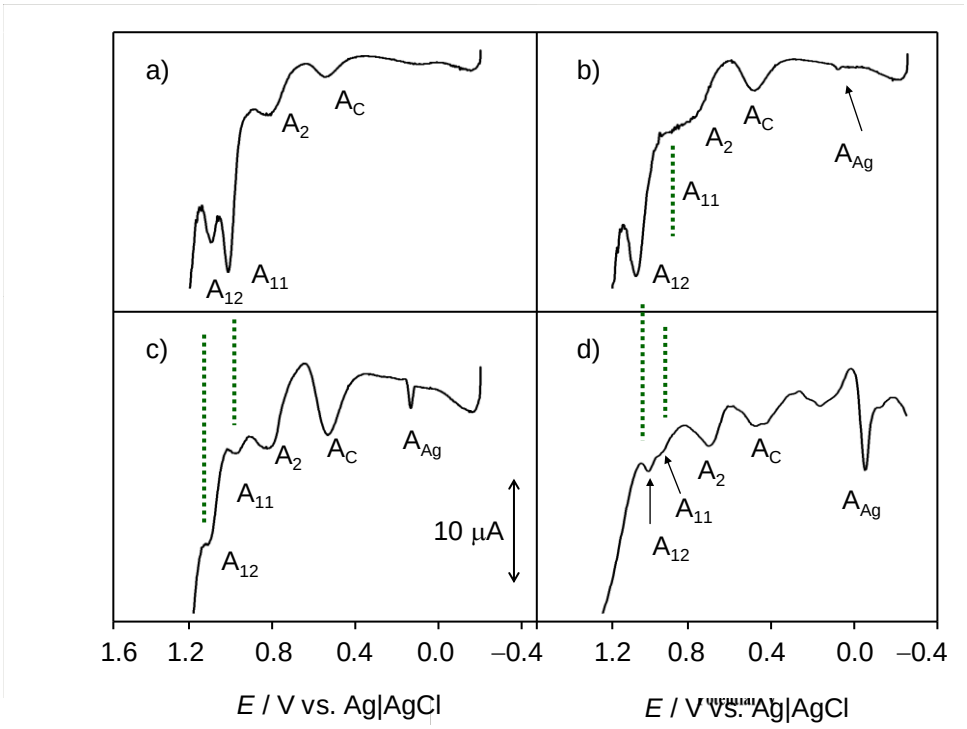

Figure 7.

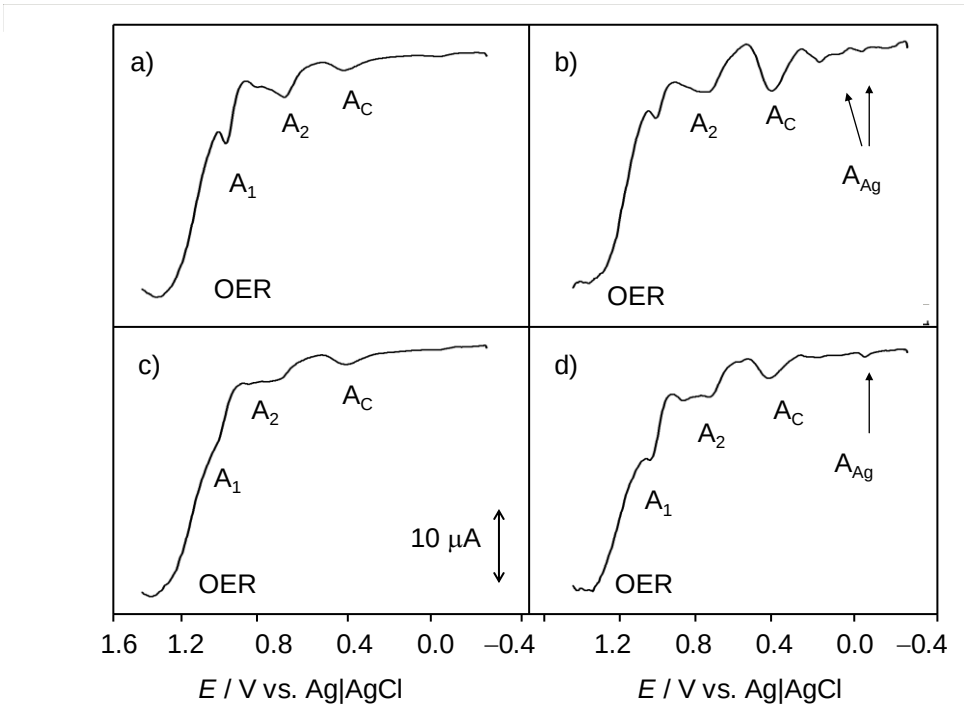
a)
b)
c)
d)
A_1
A_2
A_C
A_{Ag}
OER
10 μA
1.6 1.2 0.8 0.4 0.0 –0.4
1.2 0.8 0.4 0.0 –0.4
E / V vs. Ag|AgCl
E / V vs. Ag|AgCl

Figure 8.

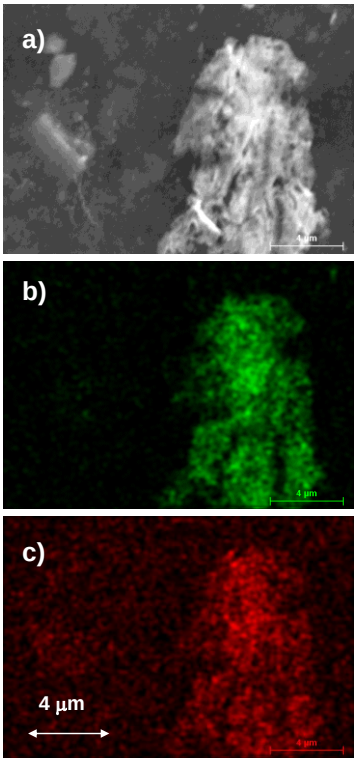

Figure 9.

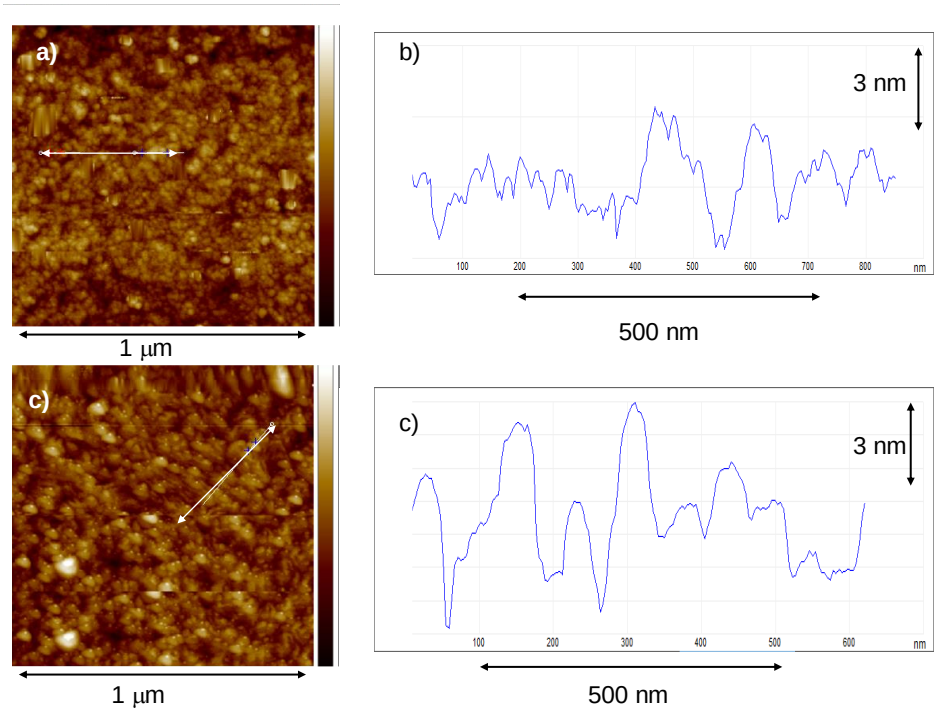
a)
1 μm
b)
3 nm
100
200
300
400
500
600
700
800
nm
500 nm
c)
1 μm
c)
3 nm
100
200
300
400
500
600
nm
500 nm

Figure 10.

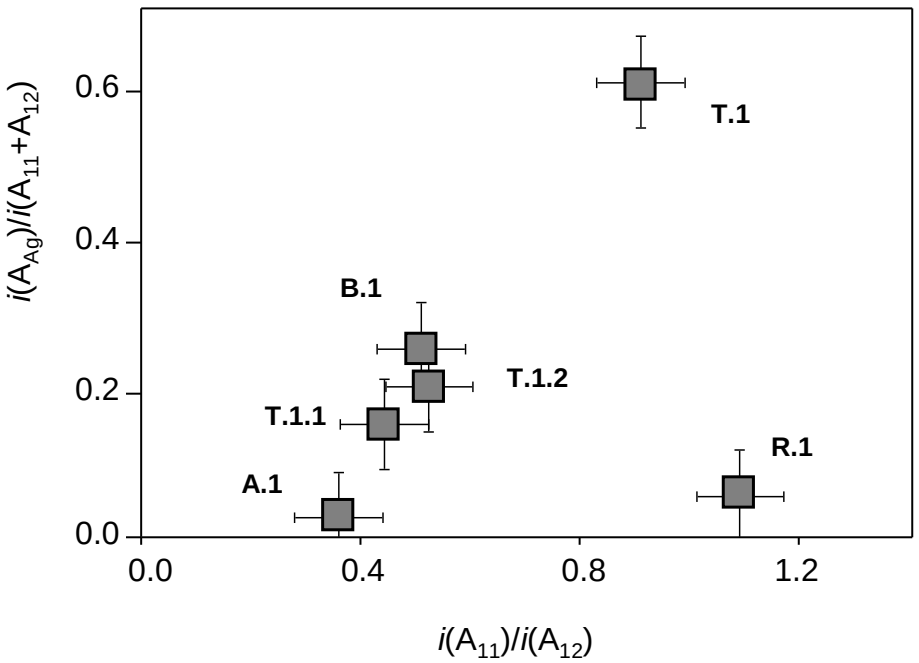

Figure 11.

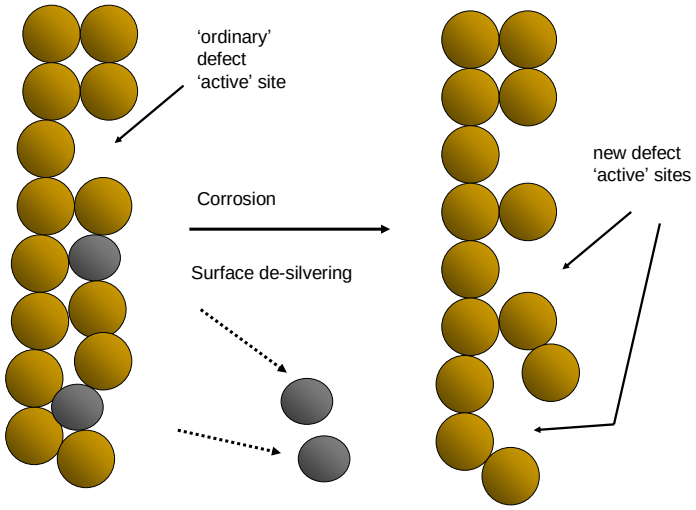
'ordinary'
defect
'active' site
Corrosion
Surface de-silvering
new defect
'active' sites

Figure 12.

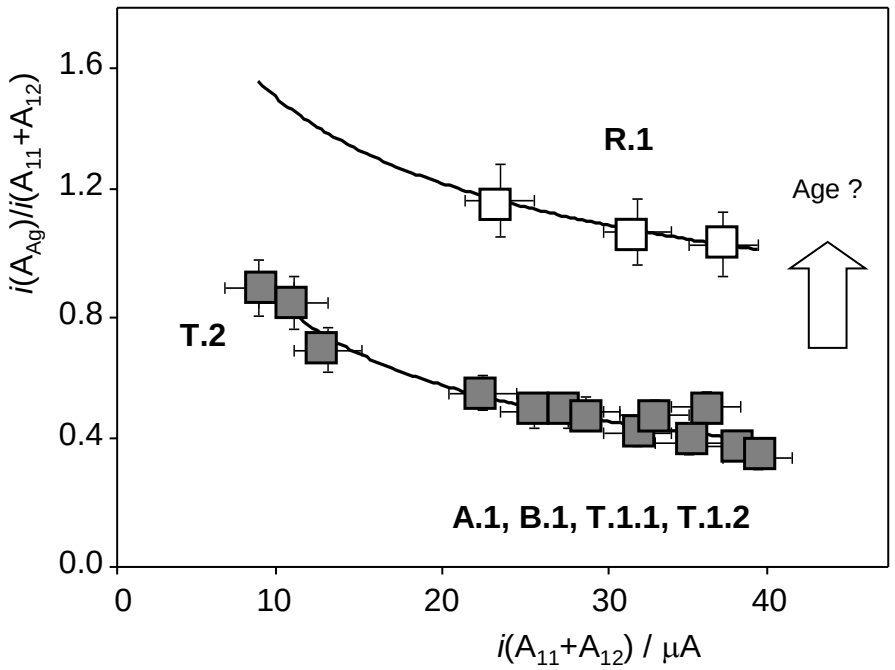
1.6
1.2
0.8
0.4
0.0
0
10
20
30
40
$i(A_{Ag})/i(A_{11}+A_{12})$
$i(A_{11}+A_{12})$ / μA
R.1
T.2
A.1, B.1, T.1.1, T.1.2
Age ?